

Influence of the temporal shape of femtosecond pulses on silicon micromachining

Tissa C. Gunaratne, Xin Zhu, Vadim V. Lozovoy, and Marcos Dantus

Citation: *J. Appl. Phys.* **106**, 123101 (2009); doi: 10.1063/1.3253330

View online: <http://dx.doi.org/10.1063/1.3253330>

View Table of Contents: <http://jap.aip.org/resource/1/JAPIAU/v106/i12>

Published by the [American Institute of Physics](#).

Related Articles

Microfabricated optofluidic ring resonator structures
Appl. Phys. Lett. **99**, 141108 (2011)

Phenomenological modeling of long range noncontact friction in micro- and nanoresonators
J. Appl. Phys. **110**, 064512 (2011)

An insulating liquid environment for reducing adhesion in a microelectromechanical system
Appl. Phys. Lett. **99**, 113516 (2011)

A robotics platform for automated batch fabrication of high density, microfluidics-based DNA microarrays, with applications to single cell, multiplex assays of secreted proteins
Rev. Sci. Instrum. **82**, 094301 (2011)

Optimizing mixing in lid-driven flow designs through predictions from Eulerian indicators
Phys. Fluids **23**, 082005 (2011)

Additional information on J. Appl. Phys.

Journal Homepage: <http://jap.aip.org/>

Journal Information: http://jap.aip.org/about/about_the_journal

Top downloads: http://jap.aip.org/features/most_downloaded

Information for Authors: <http://jap.aip.org/authors>

ADVERTISEMENT

**AIP**Advances

Submit Now

**Explore AIP's new
open-access journal**

- **Article-level metrics
now available**
- **Join the conversation!
Rate & comment on articles**

Influence of the temporal shape of femtosecond pulses on silicon micromachining

Tissa C. Gunaratne, Xin Zhu, Vadim V. Lozovoy, and Marcos Dantus^{a)}*Department of Chemistry, Michigan State University, East Lansing, Michigan 48824, USA*

(Received 16 July 2009; accepted 23 September 2009; published online 17 December 2009)

The influence of femtosecond laser pulse shaping on silicon wafer micromachining is explored. Surface second harmonic generation provides *in situ* pulse characterization of the laser pulses, and plasma and atomic emissions were identified as valuable indicators of the micromachining process. The ablation threshold was found to decrease as the bandwidth of the pulses increases, as well as for shorter pulses. Dependence of atomic and plasma emissions on temporal shape of the pulses confirmed that emission preceded ablation and has a threshold as well. The morphology of micromachined holes was observed to be dependent upon pulse duration. © 2009 American Institute of Physics. [doi:10.1063/1.3253330]

I. INTRODUCTION

There are a number of studies on the morphology of laser-ablated holes in both reactive and inert atmospheres.^{1–5} Studies have been carried out using nanosecond, picosecond, and femtosecond pulses. The heat affected zone formed by nanosecond micromachining is considered to be a drawback because it causes a number of defects including spatter, remelted layers, or microcracking.^{6,7} Femtosecond lasers produce negligible or no heating⁴ and their use for micromachining is growing in popularity.^{8,9} Our research group has made progress in controlling physicochemical processes using shaped femtosecond laser pulses^{10,11} and we have explored the effect of pulse shaping and bandwidth during the ablation of metallic substrates.¹² In this report, we explore the effect of pulse shaping on silicon wafer micromachining by systematically changing the bandwidth or spectral phase of the pulse. For diagnostic purposes, we use laser induced breakdown spectroscopy (LIBS), plasma emission (PE), and surface second harmonic generation (SSHG). The morphology of the resulting hole is evaluated by electron microscopy.

The physical mechanism for the laser ablation of metals and semiconductors with short laser pulses has been studied in detail over the recent decades. Imaging of the melting and evaporation of silicon surfaces with femtosecond laser pulses was reported by Shank and co-workers,^{13–15} who carried out optically induced reflectivity measurements using a pump-probe scheme with 90 fs pulses centered at 620 nm. Immediately following excitation with femtosecond laser pulses, reflectivity is dominated by an electron-hole (*e-h*) plasma.¹⁶ With increasing intensity, the *e-h* plasma becomes dense enough that energy is transferred into the crystal lattice, causing melting. The molten silicon phase ejects from the melted surface as nanodroplets, which atomize in several hundred picoseconds. The apparent melting threshold was indicated to be 0.1 J/cm² at 620 nm.^{13,14}

A recent study done by von der Linde and Sokolowski-Tinten,¹⁷ with energies below the plasma forma-

tion, described the ablation as a thermal process taking longer than the thermalization of absorbed energy. Although this ablation threshold (0.3 J/cm² at 620 nm, 120 fs) is higher than the ablation threshold recorded by Shank *et al.*¹⁴ (0.1 J/cm²), it involves the coexistence of gas, solid and a pressurized fluid state. We explored the effect of temporal shape and the bandwidth of ultrashort laser pulses on surface SHG generation, atomic (LIBS), and PE and on spatial characteristics of resulting micromachining. We hope that with a better understanding of the femtosecond laser ablation process these results will lead to more efficient and reproducible silicon micromachining.

II. EXPERIMENTAL

Experiments were performed using a regeneratively amplified Ti:sapphire laser system (Spectra Physics). A 128 pixel pulse shaper, located between the oscillator and amplifier, was used to correct phase distortions resulting in transform limited (TL) pulses centered at 800 nm (35 fs, 750 μJ/pulse at 1 kHz) at the sample. Our pulse shaping system is a precursor to the femtoFit (BioPhotonic Solutions, Inc.) with multiphoton intrapulse interference phase scan (MIIPS).^{18–22} MIIPS measures the spectral phase of femtosecond laser pulses and eliminates phase distortions in order to deliver well-controlled and characterized pulses at the focal plane of the microscope objective. The pulse shaper was used to introduce the different phases for evaluation purposes. A full description of the MIIPS procedure is beyond the scope of this article. Briefly, MIIPS is unlike other pulse characterization methods because it does not require interferometry or autocorrelation. Instead, it uses the dependence of nonlinear optical processes such as the spectrum of the second harmonic on a set of calibrated spectral phases in order to characterize the pulses.^{18–23}

The laser beam was focused by either a 40× objective with 0.6 numerical aperture (Plan Fluor ELWD, Nikon), or a 15× all-reflective objective with 0.28 numerical aperture (15× REFLX, Edmund Optics), or a 100 mm focal length lens. The focal plane was determined by scanning the distance between the sample and the objective. The sample was

^{a)}Electronic mail: Dantus@msu.edu.

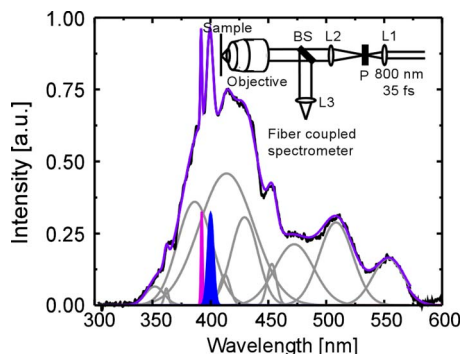


FIG. 1. (Color online) Emission spectrum recorded during Si wafer micro-machining. The data was recorded with 4.0 J/cm^2 femtosecond laser pulses. The overall emission spectrum can be decomposed into a sharp LIBS signal from atomic Si at 390.55 nm and a broader feature corresponding to the SSHG centered at 400 nm . The rest of the broad emission corresponds to a broadband PE. The inset shows the experimental setup used for this experiment. The sample was mounted on a motorized XY translational stage, L1, L2, and L3 are 300 , 600 , and 50 mm lenses, respectively, BS is a dichroic beamsplitter which transmits 800 nm and reflects from 300 to 650 nm .

mounted at normal laser incidence on a motorized X-Y translational stage that was scanned in order to introduce fresh sample per every laser shot. Before the objective, a $100 \mu\text{m}$ pinhole was placed within a two lens Keplerian telescope to spatially clean the beam before reaching the objective.

In situ monitoring of the ablation process was achieved by confocal detection of the light at 90° emitted during ablation of the Si (100) wafer surface (see Fig. 1, inset). The spectrum of this emission was detected by a thermoelectrically cooled high-sensitivity miniature spectrometer (QE 65000, Ocean Optics) and decomposed into SSHG, LIBS, and PE, as shown in Fig. 1. The laser power dependence of atomic emission lines was measured for TL pulses using a monochromator to isolate the appropriate spectral region and a photomultiplier tube. The signal was averaged using a box-car integrator.

III. RESULTS

The laser power dependence of the silicon ablation process was measured by monitoring the intensity of the LIBS atomic emission of the strongest line (390.552 nm). The threshold values obtained are low compared with metal LIBS threshold values.¹² The threshold for Si was 0.35 J/cm^2 when $\sim 35 \text{ fs}$ TL pulses are used with spectral bandwidth of 27 nm and this value is comparable to the values obtained by von der Linde and Sokolowski-Tinten¹⁷ (0.3 J/cm^2). This value is lower than the LIBS threshold for Cu (0.5 J/cm^2) and Al (0.6 J/cm^2) measured by our group.¹²

We measured the focal depth by translating the objective normal to the sample plane. This experiment showed that photoemission is strongly dependent on the location of the focus, as shown in Fig. 2. The PE [solid squares in Fig. 2(b)] forms first and at or below threshold notice that plasma signal dominates. For low laser intensity [0.4 J/cm^2 , solid squares in Fig. 2(a)] very low emission is observed when the sample plane is exactly at the focus. This is because the illuminated area is the smallest. As the power intensity increases [0.8 J/cm^2 , open circles and 8.0 J/cm^2 solid tri-

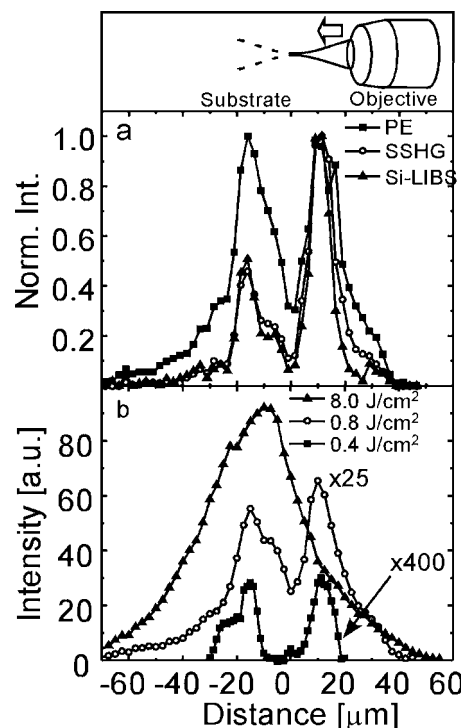


FIG. 2. Focus distance dependence. (a) Intensity for different spectral emissions [PE (■), SSHG (●), and Si-LIBS (▲)], as a function of distance from the focus recorded with 0.2 mJ/pulse . (b) Total photoemission intensity as a function of distance from the focus recorded for different pulse energies; 0.4 J/cm^2 (■), 0.8 J/cm^2 (○), and 8.0 J/cm^2 (▲). Data was obtained by moving the objective toward the sample; positive values imply the laser focuses inside the sample.

angles in Fig. 2(b)] the LIBS signal \times increases considerably. The LIBS and SSHG signals show a very similar focal spot dependence. At higher laser intensities [8.0 J/cm^2 , solid triangles in Fig. 2(b)] the PE, LIBS, and SSHG signals are maximized when the focal region is approximately $10 \mu\text{m}$ inside the sample. Note that at the higher laser intensities, one no longer observes a minimum at the focal point.

The linear chirp dependence on the Si LIBS emission was measured to find out if the effect on semiconductor substrate is similar to the effect on metallic samples.¹² The phase function for quadratic chirp is written as $\phi(\omega) = 1/2 \phi''(\omega - \omega_0)^2$. Linear chirp (ϕ'') from $-10\,000$ to $10\,000 \text{ fs}^2$ were implemented precisely using the pulse shaper with 2.0 J/cm^2 per pulse and are shown in Fig. 3. By

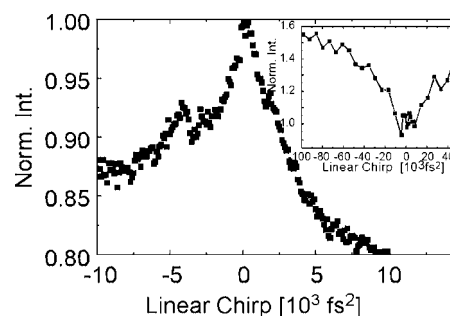


FIG. 3. Femtosecond LIBS dependence on linear chirp recorded for Si atomic emission line at 390.552 nm using MIIPS box pulse shaper with the laser intensity of 2.0 J/cm^2 . Inset shows the chirp dependence data for very large chirp values obtained by moving the compressor grating.

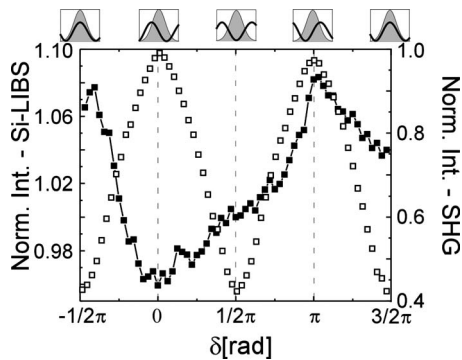


FIG. 4. Si-LIBS (■) and SHG (□) signal dependence on sinusoidal phase modulation with 2.0 J/cm^2 femtosecond laser pulses. The corresponding phase functions as a function of δ are shown in the upper insets with wavelength in X-axis (770–830 nm).

isolating the atomic emission lines from the total photoemission with a set of Gaussian functions we found that chirp could enhance or suppress LIBS signal. A much greater range of linear chirp was achieved by moving the grating position in the compressor of the laser amplifier. The overall range in this case was $-50\,000$ to $100\,000 \text{ fs}^2$. The results of these measurements (given in the inset of Fig. 3) show that for pulses with a very large chirp (when the pulses were stretched to approximately 10 ps) the LIBS signal increases by 55% compared with the signal obtained for TL pulses. The observed results are asymmetric for low chirp values, similar to those found for metal LIBS.¹² By comparison, the SHG signal decreases by a factor of 200 when the pulses have a $100\,000 \text{ fs}^2$ chirp. For long pulses, when chirp $>10\,000 \text{ fs}^2$ and corresponding duration $>1 \text{ ps}$, LIBS emission depends only on pulse duration and is therefore symmetric with respect to the chirp value. For shorter pulses, when chirp $<10\,000 \text{ fs}^2$ and pulse duration is $<1 \text{ ps}$, the dependence of chirp is asymmetric, and the shape of the pulse can make a 10%–20% difference on the LIBS signal.

The dependence of the LIBS signal on a sinusoidal phase modulation was also measured. These experiments were inspired by MII theory.²¹ The ability of sine phase modulation to control multiphoton processes on molecules, proteins, and nonlinear crystals^{24–27} is well documented. Here, we are trying to find the link between multiphoton processes that are involved in the laser matter interaction and ablation of atoms from the sample surface to give a LIBS signal. The measurements were carried out by introducing phase functions in the frequency (ω) domain defined by $\phi = \alpha \sin[\gamma(\omega - \omega_0) - \delta]$, where γ is the bandwidth of the pulse (35 fs) and δ determines the position of the mask with respect to the spectrum of the pulse. The resulting LIBS signal is plotted as a function of δ in Fig. 4 (solid squares) along with SHG signal generated using a nonlinear crystal for comparison (open squares). This experiment was performed with pulse energies of 2.0 J/cm^2 , and by deconvoluting atomic emission lines with Gaussian fitting, the changes observed in the LIBS emission were modest ($\sim 10\%$). One important observation is that the signal is not symmetric and does not track the generation of SSHG in the sample (see Fig. 4). This

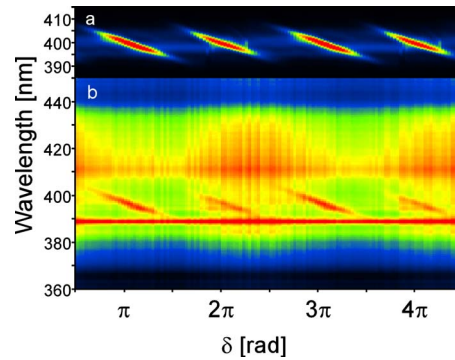


FIG. 5. (Color online) Si-LIBS and SSHG spectra obtained by applying sinusoidal modulation are plotted as 2D maps with 2.0 J/cm^2 femtosecond laser pulses. Panel (a) shows a typical MIIPS trace obtained with a SHG crystal, and panel (b) shows all the emission components observed under micromachining conditions, including the broad plasma, the SSHG features which are similar to those in panel (a) and the Si atomic emission.

contrasts with the results obtained for metals when the signal was symmetric around $\delta = \pi/2$ with time ordering of the pulses.

SSHG was first reported by Terhune *et al.*²⁸ in calcite. A theoretical discussion of this phenomenon was reported soon after by several research groups as a quadrupolar type of interaction^{29,30} including the involvement of free electrons.³¹ SSHG from silicon and germanium was first reported by Bloembergen and Chang³² in 1966 with a subsequent report on an experimental method to detect SSHG.³³ Shank *et al.*¹³ has shown that SSHG has two main sources, anisotropic and isotropic with respect to polarization. No effort was made here to measure the polarization dependence of the photoemission.

As mentioned in Sec. II, our group developed a method called MIIPS²¹ for accurately characterizing the spectral phase of the femtosecond laser by introducing a well-calibrated reference phase function and measuring changes in the SHG spectrum. We have found that SSHG similarly tracks the changes, as shown in Fig. 5. This is a valuable observation as it allows us to determine the spectral phase of the pulse after passing through a high numerical aperture objective interacting with the sample *in situ* on the surface of ablation.²³

The SSHG signal magnitude is comparable to Si-LIBS and PE. When a sinusoidal modulation is introduced, the same second harmonic modulation was observed as in a nonlinear crystal. This phenomenon is common in all the phase functions that were tested, but is more prominent in sinusoidal modulation, and duplicates the MIIPS trace for TL pulses. The MIIPS trace for a nonlinear crystal is given in Fig. 5(a) and LIBS spectra are given in Fig. 5(b). They are plotted as three-dimensional (3D) maps with the scanning parameter δ on the X-axis and wavelength on the Y-axis, with intensity being color-coded (red-high intensity and black/blue-low intensity).

For the MIIPS measurements, we use the function $f(\omega) = \alpha \sin(\gamma\omega - \delta)$ to generate reference functions in the frequency domain (ω). Scanning the parameter δ from 0 to 4π and collecting the SHG spectrum for each value generates two replicas of the two-dimensional MIIPS trace from which

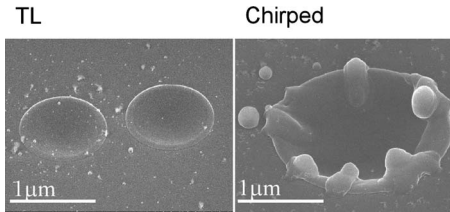


FIG. 6. Effect of phase modulation on the morphology of micromachined features obtained on Si (100) wafer (scale bar=1 μm) with 0.35 J/cm² femtosecond laser pulses. Images shown here are obtained with TL pulses (35 fs) and highly chirped pulses (60 000 fs², equivalent to 1 ps). Other conditions including power and focus are the same for both experiments. Notice the extensive melting associated with the hole made with chirped pulses.

one can find the condition $\delta_{\text{max}}(\omega)$ when the maximum SHG signal is obtained [see Fig. 5(a)], note that each of the four features is separated by π for TL pulses. The position and shape of the MIIPS features can be used for *in situ* characterization and compensation of the spectral phase of the pulse that interacts with silicon substrate.¹⁹

The effect of pulse shaping on the morphology of drilled holes was investigated using two different phase shapes as a proof of principle experiment. In this particular experiment, TL (35 fs) pulses and highly chirped ($-60\,000\text{ fs}^2$, equivalent to 1 ps) pulses were used with a 40x objective. The SEM images are shown in Fig. 6. It is clear that TL pulses give clean features compared with highly chirped pulses, where melting can clearly be seen. These images imply that the greater LIBS signal observed for large chirp values results from increased melting which then leads to evaporation.

IV. DISCUSSION

Results from our study confirm that the threshold for obtaining a LIBS signal from silicon using TL pulses is around 0.35 J/cm² (Fig. 7), and this value is smaller than the thresholds recorded for metallic samples; 0.5 and 0.6 J/cm² for Cu and Al, respectively.¹² The higher threshold for metals compared with silicon could be rationalized by the idea that thresholds are higher in materials in which the deposited energy is rapidly carried away from the surface and redistributed over a large area.¹⁷ Alternatively, silicon absorbs light at the laser wavelength used here while the metals do not.

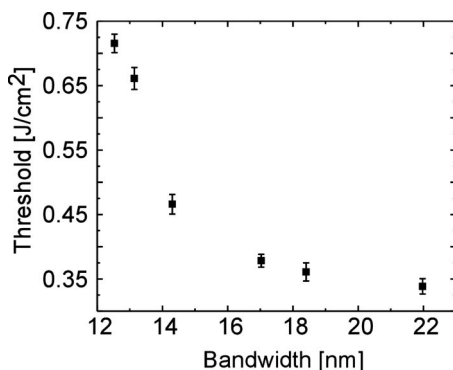


FIG. 7. The LIBS power threshold dependence on the bandwidth of the laser pulse (full-width at half maximum). Each data point is an average of 5 experimental measurements.

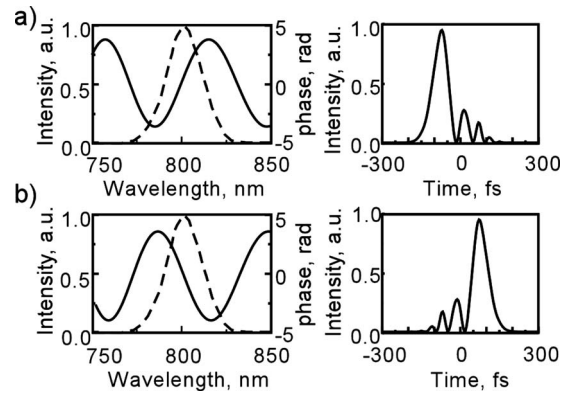


FIG. 8. Temporal profile of the pulses with sinusoidal phase function $\phi = \pi \sin[35\text{ fs}(\omega - \omega_0) - \delta]$ when $\delta = \pi$ (a) and $\delta = 0$ (b). Left column: spectral power (dashed line) and phase (solid line); right column: calculated time profile of the intensity.

The effect of sinusoidal phase modulation on the LIBS signal was found to be different from the dependence of SSHG. For SSHG intensity a maximum is reached every time for $\phi = \pi \sin[35\text{ fs}(\omega - \omega_0) - n\pi]$; however the LIBS signal reaches a minimum when n is even, and a maximum when n is odd. This difference can be explained by understanding the temporal progression of the pulse shown in Fig. 8. Notice that for (a) $\phi = \pi \sin[35\text{ fs}(\omega - \omega_0) - \pi]$, the pulse starts with a fast-rising intense laser pulse that exceeds the ablation threshold; the subsequent subpulses continue to provide energy for the ablation process. In contrast, for (b) $\phi = \pi \sin[35\text{ fs}(\omega - \omega_0)]$, the pulse starts with low energy subpulses that are below threshold, and their energy is wasted. The LIBS signal dependence on the sinusoidal phase modulations shows a distinctive dependence contrast to metallic samples.¹²

When we tested linear chirp from $-10\,000$ to $10\,000\text{ fs}^2$, TL pulses were found to yield slightly higher LIBS signal. Interestingly, larger chirp values resulted in even greater LIBS signal. When the pulse duration reached $\sim 8\text{ ps}$, the signal amplitude had increased by about 55%. It is important to note that the interaction of femtosecond pulses with Si substrate involves a melted surface layer.¹⁶ When pulses facilitate surface melting, for example longer laser pulses that result from large chirp values, the LIBS signal increases compared with TL pulses.

The strong dependence of PE on focal spot distance can be very useful for micromachining. The PE can be observed in near- and above-threshold conditions, and can be very useful in creating submicron features on Si-wafers as photoemission is minimal at the focal point when the laser fluence is close to the ablation threshold. LIBS and SSHG signals appear slightly above the threshold fluence for PE, with a minima at the focal point.

SSHG has been observed from silicon surfaces before, but to our knowledge, this phenomenon has never been used to aid in micromachining. The signal amplitude is comparable to LIBS signal and can be observed above threshold fluences. SSHG may have much wider implications as the phenomenon can be utilized for the compensation of femtosecond laser pulses at samples where a nonlinear crystal can-

not be used to determine the spectral phase of the pulse *in situ*. Further, SSHG can be used to monitor the spectral phase of the femtosecond laser pulse interacting with the sample.

Surface modifications on drilled surfaces with either single or multiple pulses have been a concern for precision micromachining and include features such as irregular columns and ripples. These surface modifications occur when molten silicon forms, a process that requires absorption of the laser pulse and thermalization. This process can last up to a few nanoseconds depending on the laser fluence.¹⁷ The use of a two pulse sequence was introduced as a way to avoid deformation, mainly ripples, due to the fluid dynamics of molten silicon on the ablated area. The two pulses were separated by a few picoseconds either using a pump-probe scheme³⁴ or using pulse shaping techniques.^{2,35}

V. CONCLUSIONS

We explored laser pulse characteristics for reproducibility and improved silicon micromachining. Three different emissions were used for monitoring the laser pulse interaction, surface SHG, atomic emission, and PE. As the bandwidth of the laser pulse increases, the threshold for atomic emission decreases. This effect is even more pronounced than that observed for metallic samples. This conclusion is based upon the fact that when we stretched 35 fs laser pulses up to 8ps the atomic emission increased by 55%. The sinusoidal phase modulation shows sharp deviation from metallic samples in which the LIBS signal is symmetric around TL pulses. For silicon, the atomic emission signal was found to depend on the sign of the sinusoidal phase modulation because the ablation of silicon has to first reach a threshold value which is probably associated with ionization.

The PE as a function of distance from the focal spot was found to be a valuable parameter to determine the focal plane, this dependence should be useful for machining nanometer sized features at the focus with near threshold energies. Surface second harmonic generation was found to require higher fluences. Low energy TL pulses minimize the melting to produce clean features, as confirmed by electron microscope images from single laser shots. For shorter pulses (<1 ps) temporal shaping can be used to optimize the ablation process.

ACKNOWLEDGMENTS

We gratefully acknowledge funding from the Chemical Sciences, Geosciences, and Biosciences Division, Office of Science, U.S. Department of Energy Contract No. DE-FG02-01ER15143. We would like to thank Chris Cowen and Dr. Marty Crimp, Department of Electrical Engineering, and MSU for helping with SEM imaging. We are thankful for the participation of Raj Amin who was supported by the High

School Honors Science Mathematics Engineering Program at MSU.

- ¹J. Bonse, S. Baudach, J. Kruger, W. Kautek, and M. Lenzner, *Appl. Phys. A: Mater. Sci. Process.* **74**, 19 (2002).
- ²V. Hommes, M. Miclea, and R. Hergenroder, *Appl. Surf. Sci.* **252**, 7449 (2006).
- ³A. Borowiec, M. Mackenzie, G. C. Weatherly, and H. K. Haugen, *Appl. Phys. A: Mater. Sci. Process.* **76**, 201 (2003).
- ⁴M. S. Amer, M. A. El-Ashry, L. R. Dosser, K. E. Hix, J. F. Maguire, and B. Irwin, *Appl. Surf. Sci.* **242**, 162 (2005).
- ⁵B. C. Stuart, M. D. Feit, S. Herman, A. M. Rubenchik, B. W. Shore, and M. D. Perry, *J. Opt. Soc. Am. B* **13**, 459 (1996).
- ⁶A. Cocoran, L. Sexton, B. Seaman, P. Ryan, and G. Byrne, *J. Mater. Process. Technol.* **123**, 100 (2002).
- ⁷J. Jandeleit, A. Horn, R. Weichenhain, E. W. Kreutz, and R. Poprawe, *Appl. Surf. Sci.* **127**, 885 (1998).
- ⁸B. Rethfeld, K. Sokolowski-Tinten, D. von der Linde, and S. I. Anisimov, *Appl. Phys. A: Mater. Sci. Process.* **79**, 767 (2004).
- ⁹S. K. Sundaram and E. Mazur, *Nature Mater.* **1**, 217 (2002).
- ¹⁰M. Dantus and V. V. Lozovoy, *Chem. Rev. (Washington, D.C.)* **104**, 1813 (2004).
- ¹¹V. V. Lozovoy and M. Dantus, *Annu. Rep. Prog. Chem., Sect. C: Phys. Chem.* **102**, 227 (2006).
- ¹²T. Gunaratne, M. Kangas, S. Singh, A. Gross, and M. Dantus, *Chem. Phys. Lett.* **423**, 197 (2006).
- ¹³C. V. Shank, R. Yen, and C. Hirlimann, *Phys. Rev. Lett.* **51**, 900 (1983).
- ¹⁴C. V. Shank, R. Yen, and C. Hirlimann, *Phys. Rev. Lett.* **50**, 454 (1983).
- ¹⁵M. C. Downer, R. L. Fork, and C. V. Shank, *J. Opt. Soc. Am. B* **2**, 595 (1985).
- ¹⁶D. H. Auston and C. V. Shank, *Phys. Rev. Lett.* **32**, 1120 (1974).
- ¹⁷D. von der Linde and K. Sokolowski-Tinten, *Appl. Surf. Sci.* **154-155**, 1 (2000).
- ¹⁸Y. Coello, V. V. Lozovoy, T. C. Gunaratne, B. W. Xu, I. Borukhovich, C. H. Tseng, T. Weinacht, and M. Dantus, *J. Opt. Soc. Am. B* **25**, A140 (2008).
- ¹⁹V. V. Lozovoy, I. Pastirk, and M. Dantus, *Opt. Lett.* **29**, 775 (2004).
- ²⁰M. Dantus, V. V. Lozovoy, and I. Pastirk, *Laser Focus World* **43**, 101 (2007).
- ²¹B. Xu, J. M. Gunn, J. M. Dela Cruz, V. V. Lozovoy, and M. Dantus, *J. Opt. Soc. Am. B* **23**, 750 (2006).
- ²²I. Pastirk, B. Resan, A. Fry, J. MacKay, and M. Dantus, *Opt. Express* **14**, 9537 (2006).
- ²³X. Zhu, T. C. Gunaratne, V. V. Lozovoy, and M. Dantus, *Opt. Express* **15**, 16061 (2007).
- ²⁴V. V. Lozovoy, I. Pastirk, K. A. Walowicz, and M. Dantus, *J. Chem. Phys.* **118**, 3187 (2003).
- ²⁵I. Pastirk, J. M. Dela Cruz, K. A. Walowicz, V. V. Lozovoy, and M. Dantus, *Opt. Express* **11**, 1695 (2003).
- ²⁶J. M. Dela Cruz, I. Pastirk, V. V. Lozovoy, K. A. Walowicz, and M. Dantus, *J. Phys. Chem. A* **108**, 53 (2004).
- ²⁷K. A. Walowicz, I. Pastirk, V. V. Lozovoy, and M. Dantus, *J. Phys. Chem. A* **106**, 9369 (2002).
- ²⁸R. W. Terhune, P. D. Maker, and C. M. Savage, *Phys. Rev. Lett.* **8**, 404 (1962).
- ²⁹P. S. Pershan, *Phys. Rev.* **130**, 919 (1963).
- ³⁰E. Adler, *Phys. Rev.* **134**, A728 (1964).
- ³¹N. Bloembergen, *Proc. IEEE* **51**, 124 (1963).
- ³²N. Bloembergen and R. K. Chang, in *Proceedings of the Physics of Quantum Electronics Conference*, edited by P. L. Kelley, B. Lax, and P. E. Tannenwald (McGraw-Hill, New York, 1966), p. 80.
- ³³N. Bloembergen, R. K. Chang, S. S. Jha, and C. H. Lee, *Phys. Rev.* **174**, 813 (1968).
- ³⁴T. Y. Choi, D. J. Hwang, and C. P. Grigoropoulos, *Appl. Surf. Sci.* **197-198**, 720 (2002).
- ³⁵D. Pestov, V. V. Lozovoy, and M. Dantus, *Opt. Express* **17**, 14351 (2009).